Editors' Suggestion | Featured in Physics

Shear-Induced Gelation of Self-Yielding Active Networks

David A. Gagnon,[1,†] Claudia Dessi,[1,†] John P. Berezney,[2] Remi Boros,[3] Daniel T.-N. Chen,[2] Zvonimir Dogic,[3] and Daniel L. Blair[1,*]

[1]*Department of Physics and Institute for Soft Matter Synthesis & Metrology, Georgetown University, 3700 O Street NW, Washington, D.C. 20057, USA*

[2]*Department of Physics, Brandeis University, Waltham, Massachusetts 02453, USA*

[3]*Department of Physics, University of California Santa Barbara, Santa Barbara, California 93106, USA*

(Received 28 July 2020; accepted 14 September 2020; published 22 October 2020)

An enticing feature of active materials is the possibility of controlling macroscale rheological properties through the activity of the microscopic constituents. Using a unique combination of microscopy and rheology we study three dimensional microtubule-based active materials whose autonomous flows are powered by a continually rearranging connected network. We quantify the relationship between the microscopic dynamics and the bulk mechanical properties of these nonequilibrium networks. Experiments reveal a surprising nonmonotonic viscosity that strongly depends on the relative magnitude of the rate of internally generated activity and the externally applied shear. A simple two-state mechanical model that accounts for both the solidlike and yielded fluidlike elements of the network accurately describes the rheological measurements.

DOI: 10.1103/PhysRevLett.125.178003

Molecular-motor generated active stresses drive the cytoskeleton away from equilibrium, endowing it with tunable mechanical properties that are essential for diverse functions such as cell division and motility [1–5]. Designing cytoskeletal biomimetic systems is a key prerequisite for creating active matter that can emulate cellular functions [6,7]. These long-term goals require quantitative understanding of how motor-generated stresses tune the mechanics of filamentous networks [8–11]. In microtubule-based active matter, kinesin motors generate extensile motion that leads to persistent breaking and reforming of the network's links [12,13]. We study how such microscopic dynamics modifies the network's mechanical properties, uncovering that the network viscosity first increases with the imposed shear rate before transitioning back to a low-viscosity state. The speed of molecular motors controls the nonmonotonic shear-dependent viscosity. A two-state phenomenological model that incorporates liquid- and solidlike elements quantitatively relates the shear-rate-dependent viscosity to locally measured flows. Our study shows that rheology of extensile networks are different from previously studied active gels [9,14], where contractility enhances mechanical stiffness. Moreover, the flow induced gelation is not captured by the continuum models of hydrodynamically interacting swimmers [15–22].

We study isotropic active networks composed of filamentous microtubules (MTs), kinesin motor complexes, and a depleting polymer that bundles MTs [12]. Kinesin clusters bind to and step along multiple MTs, generating bundle buckling and fraying (Supplemental Material, Movies S1–S3 [23]). Frayed bundles rapidly reincorporate into the network, forming new filamentous paths that continuously reconfigure the structure of the percolating network and generates turbulent flows [Figs. 1(a) and 1(b)]. Several features make such networks ideal to study influence of activity on mechanics. First, the rate of network rearrangements can be tuned by adenosine triphosphate (ATP), which determines the kinesin stepping speed [30]. Second, the efficient kinesin motors sustain steady-state active dynamics for hours [Fig. 1(c)]. Third, MT networks can be assembled on macroscopic, milliliter-scale quantities. However, rheological characterization of these materials is challenging due to very low MT volume fractions, $\phi = 0.01$ wt%. To overcome this obstacle we pushed the limits of the instrument sensitivity by designing custom rheological tools (Supplemental Material [23], Fig. 1). When combined with the ability to prepare large samples that sustain nonequilibrium activity for multiple hours, this advance enabled quantitative rheological characterization.

Measurements revealed that the sample viscosity η, exhibits a pronounced nonmonotonic dependence on the applied shear rate $\dot{\gamma}$. For small $\dot{\gamma}$, the active networks shear-thickened, with viscosity, η, increasing sharply and reaching a peak, followed by a shear-thinning response [Fig. 1(d), Supplemental Material [23], Fig. 2]. The characteristic shear rate, $\dot{\gamma}_c$, signifies the peak in the viscosity that separates the shear-thickening from the shear-thinning regime. Experiments at different ATP concentrations revealed that the motor-generated dynamics tunes the network viscosity. In the shear-thickening regime, changing ATP concentration modified viscosity by up to an order

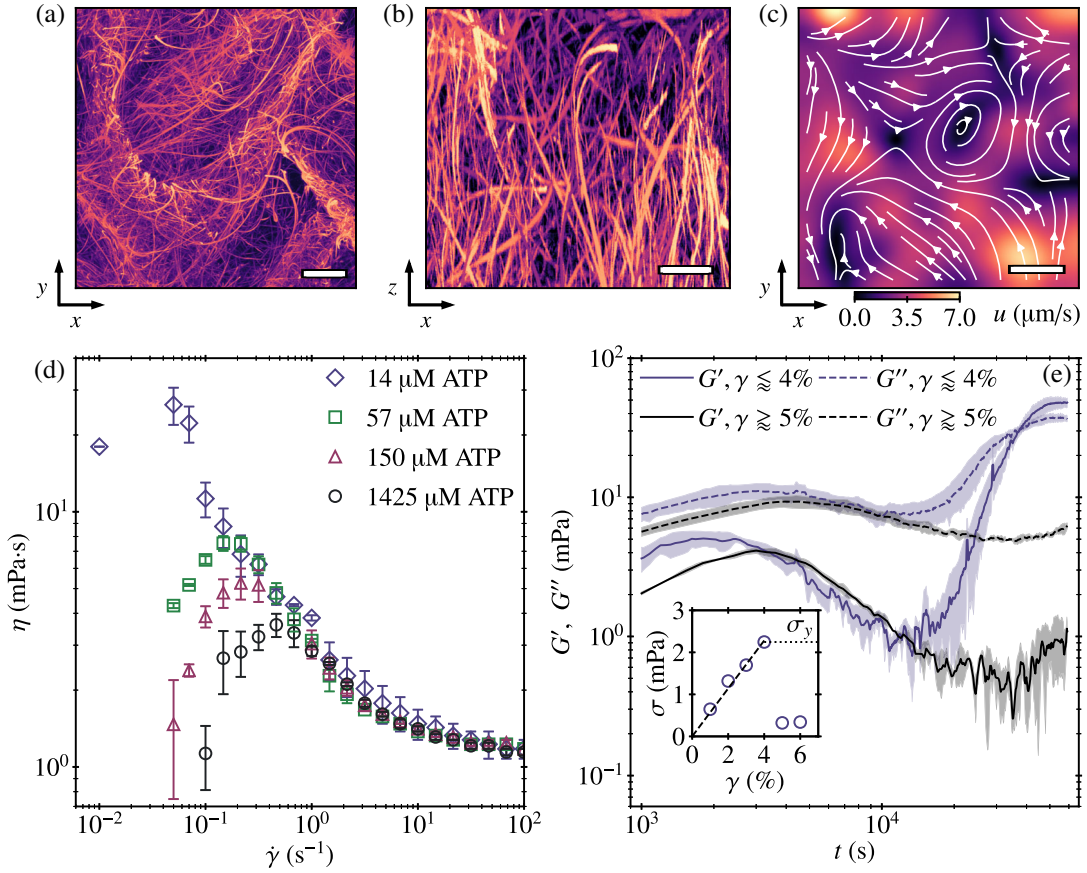

FIG. 1. Structure, dynamics, and rheology active gels. (a),(b) Confocal fluorescence images of active network in the x, y (velocity, vorticity) plane and the x, z (velocity, gradient) plane as the ATP concentration is depleted. Images represent 100 μm maximum projections. (c) Velocity field of autonomous flows and streamlines in the flow-vorticity plane with no applied shear. (d) Apparent viscosity η as a function of shear rate $\dot{\gamma}$; error bars reflect standard error across multiple samples ($N = 3$). (e) Storage G' and loss G'' moduli of network initially with $c_{\mathrm{ATP}} = 14$ μM suspension as ATP. Frequency is fixed $\omega = 1.0$ rad s^{-1}. The light colored curves indicate the oscillatory tests below yield stress σ_y, and the dark curves are above σ_y. Shading indicates the standard deviation for three experiments. Inset: stress measurements from a strain sweep provide an approximate yield stress $\sigma_y = 2.2$ mPa. Scale bars are 50 μm.

of magnitude. Conversely, in the shear-thinning regime above $\dot{\gamma}_c$, the sample viscosity was ATP independent, with all measurements collapsing on each other. ($\dot{\gamma}_c$) increased with increasing ATP concentration, while the maximum viscosity simultaneously decreased.

To explain the nonmonotonic viscosity, we note that the kinesin clusters have a dual role in the network dynamics by both generating active stresses and by passively cross-linking MTs. Processive kinesin motors take many successive 8 nm steps along a MT [31]. The motion consists of fast, tens of microseconds long power strokes that are interspersed by extended millisecods long pauses during which the kinesin is bound to a MT but at rest. The ATP concentration, the direction and the magnitude of the applied load determine the duration of the dwell times between the rapid steps [31,32], thus controlling whether a kinesin cluster predominantly generates active stress or acts as a passive cross-linker. In the absence of ATP, motors permanently link the microtubule network [Supplemental Material [23], Fig. 3(a)].

To demonstrate the dual role of kinesin clusters, we measured the rheology as the network was depleted from ATP, during which the dwell times became longer and the dominant role of clusters switched from active stress generation to passive cross-linking (Movies S2,S3 [23]). The resulting changes in the network's mechanical properties were quantified using oscillatory rheology which continuously measured the elastic G' and loss modulus G'' at a fixed frequency and amplitude [Fig. 1(e)]. The initial response was viscous dominated ($G'' > G'$), indicating that motor-generated active stresses fluidize the network. As ATP was depleted, the elastic modulus increased, eventually dominating the loss modulus ($G' > G''$), confirming the hypothesis that clusters crosslink adjoining microtubule bundles (Supplemental Material [23], Fig. 3). Rheology of ATP-depleted networks is similar to previously studied cross-linked biofilaments [33,34]. Confocal images of the ATP-depleted network show that bundles connect the rheometer's surfaces (parallel plates), giving rise to an elastic modulus [Fig. 1(b)]. Performing a fixed-

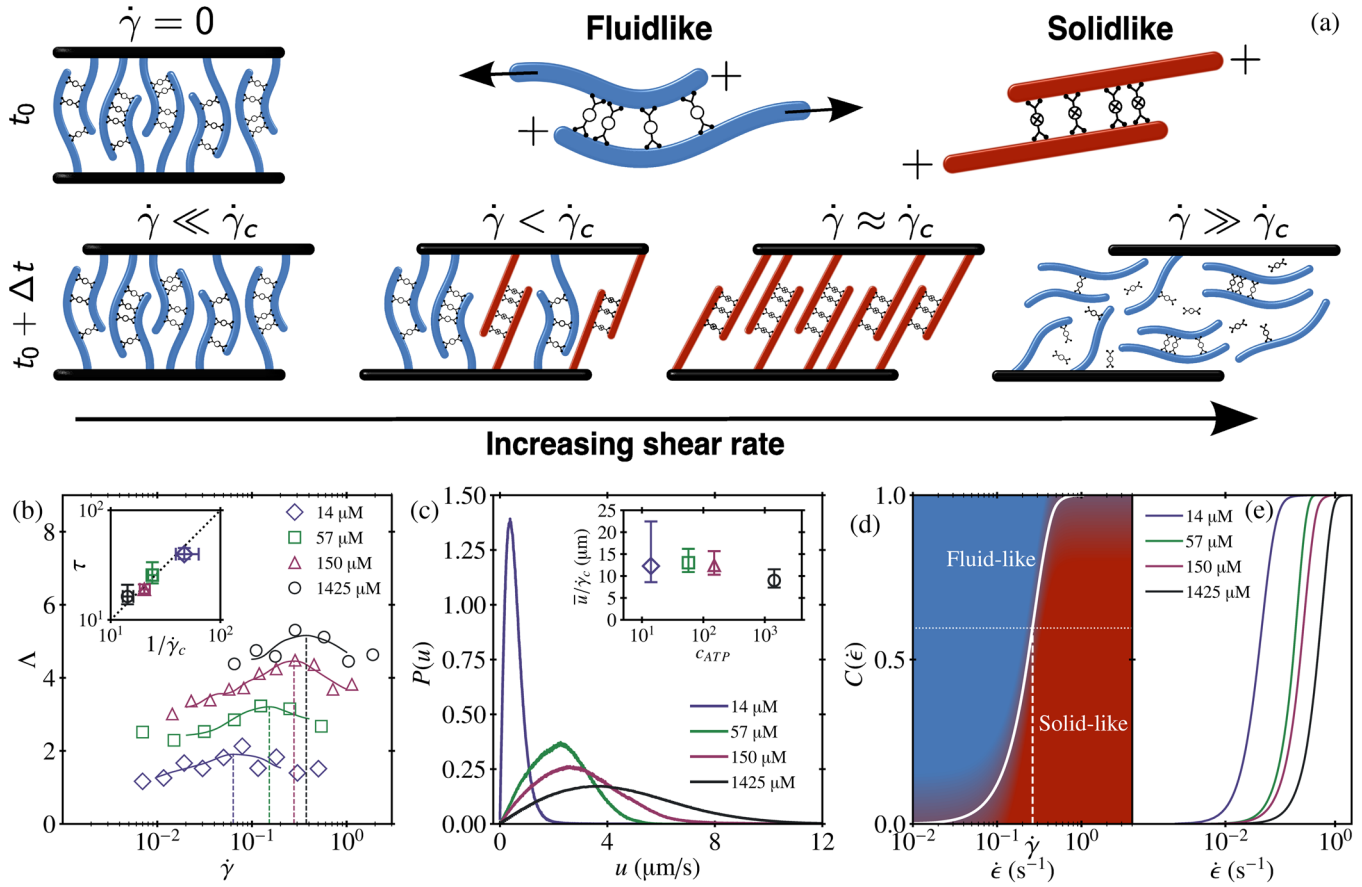

FIG. 2. Microscopic model of active self-yielding solids. (a) A sheared active network is composed of liquidlike (blue) and solidlike (red) extensile elements. The fraction of each element depends on the speed of intrinsic extension and the magnitude of the applied shear. Close to $\dot{\gamma}_c$ the speed of the boundary is comparable to the speed of the extending elements, which became taught and contribute to shear stress. Above $\dot{\gamma}_c$ the extending elements break immediately. (b) Ratio of characteristic length scales in the shear and vorticity directions; a vertical shift is introduced for clarity. Inset: the active timescale τ, measured via MT dynamics, is directly correlated to the rheological timescale $1/\dot{\gamma}_c$, dashed line is a fit of slope unity. (c) Probability distribution functions of MT speeds for different c_{ATP}. Inset: $\bar{u}/\dot{\gamma}_c$ is independent of c_{ATP}. (d) The fraction of stiffened elements is set by evaluating the cumulative distribution of sliding rates $C(\dot{\epsilon})$ at the shear rate $\dot{\gamma}$. (e) $C(\dot{\epsilon})$ for all c_{ATP}.

frequency strain amplitude sweep revealed the yield stress of the ATP-depleted network. Above a critical amplitude $\gamma_y \approx 4\%$, the elastic network broke down at a stress $\sigma_y = 2.2$ mPa. The measured stress σ increases linearly with the imposed strain, resulting in an elastic modulus of ~60 Pa, consistent with the elastic modulus of fully ATP depleted network [Fig. 1(e), Supplemental Material [23], Fig. 5).

To gain insight into our rheological measurements we note that in static situations, thin filaments can carry large tensile loads, but easily buckle under compressive axial stresses. In a dynamical case, where both the filament is extending and the boundaries are moving, filament's ability to sustain loads will depend on the relative speeds of the two dynamical elements. Motivated by these considerations, we hypothesize that sheared MT networks can be described by two mechanical states, a soft solidlike element with a finite yield stress that coexists with a fluidlike element [Fig. 2(a)]. The relative fraction of these states is set by the two competing rates that characterize the system dynamics; one rate is determined by the externally applied shear, while the other is controlled by the ATP-dependent internal rate of network rearrangements. Analogous to the static case mentioned above, network elements that extend at rates faster than the externally applied deformation self-yield and do not contribute elastically. Conversely, elements whose extensile sliding rates are slower than the externally imposed rates resist the shear and contribute elastically.

At very low shear rates ($\dot{\gamma} \ll \dot{\gamma}_c$) the entire system continuously self-yields and the fluidlike elements dominate the mechanical response. When approaching the characteristic shear rate ($\dot{\gamma} \approx \dot{\gamma}_c$), the imposed rate becomes larger than the intrinsic extensile sliding rate, leading to an increased fraction of elements being taut and elastically resisting the imposed deformation. Once they reach their yield strain, they break. Simultaneously, the internal activity leads to formation of new extending elements.

The continuous breakage and reformation of bundles produces a constant fraction of solidlike bundles that resist shear, thus increasing the effective sample viscosity. Such a state is reminiscent of conventional soft solids; elastic materials that have a high shear viscosity due to the continuous formation and breakage of elastic bonds [35]. Finally, when $\dot{\gamma} > \dot{\gamma}_c$, the imposed shear rate is larger than the extensile sliding rate of all network elements, resulting in their immediate breakage. The model predicts that solidlike elements behave elastically at $\dot{\gamma}_c$, resulting in an effective increase in stress for $\dot{\gamma} < \dot{\gamma}_c$. The network elements break at the yield stress of the inactive MT gel [Fig. 1(e), inset], determining the rheological response at $\dot{\gamma} > \dot{\gamma}_c$. Prior to breaking, taut filaments microscopically appear solidlike, with increasingly correlated velocities in the shear direction, as has been observed for other yield-stress materials such as dense emulsions [36].

To test our hypothesis, we first quantify shear dependence of velocity fields to identify microscopic signatures of shear-induced network solidification. Particle imaging velocimetry (PIV) revealed the flows fields in the reference frame where the average flow is subtracted (Supplemental Material [23], Fig. 3). From here, we determine the velocity autocorrelation lengths both in the direction parallel to and perpendicular to the flow (Supplemental Material [23], Fig. 4). Their ratio, Λ is a nonmonotonic function of $\dot{\gamma}$ with an ATP dependent peak [Fig. 2(b)]. The peak in Λ defines a timescale τ that is linearly correlated with the independently measured characteristic shear rate $\dot{\gamma}_c$ where the sample viscosity is maximum [Fig. 2(b), inset]. As the system becomes more solidlike at $\dot{\gamma}_c$, the range of the velocity correlations in the direction of shear flow increases as the filaments begin to span the system and align along the principle shear axis [36].

Next, we compared the external and internal rates to determine the fraction of solidlike elements. In the absence of an imposed shear PIV determines the distribution of microscopic strain rates generated by the autonomous flows [Fig. 2(c), Movies S4, S5]. The mean speed, $\bar{u}$, increased with increasing ATP concentration. Dividing the average speed of the unsheared network with the characteristic shear rate results in an ATP-independent length scale $\bar{u}/\dot{\gamma}_c \sim 12\ \mu$m, providing a connection between internal speeds and external shear rates [Fig. 2(c), inset]. We interpret this length scale as the average distance that microtubule filaments of opposite polarity travel prior to losing mechanical contact. Using this length scale we map internal speeds onto effective active rates. Assuming that the distribution of MT speeds is proportional to the distribution of extensile sliding rates, $P(\dot{\epsilon}) \propto P(u)$, we define $\dot{\epsilon} = u/(\bar{u}/\dot{\gamma}_c)$ using the ATP-independent proportionality constant. The fraction of slowly sliding elements in the network is estimated from the cumulative distribution function of the extensile sliding rates $C(\dot{\epsilon}) = \int_0^{\dot{\epsilon}} P(\tilde{\dot{\epsilon}})d\tilde{\dot{\epsilon}}$ [Fig. 2(d)]. The numerical value of $C(\dot{\epsilon})$ provides the fraction of solidlike elements when evaluated at $\dot{\epsilon} = \dot{\gamma}$. For a given ATP concentration, we denote this fraction at a particular shear rate as $C(\dot{\gamma})$ [Fig. 2(d)]. With increasing ATP concentration, the cumulative distribution shift to higher strain rates [Fig. 2(e)].

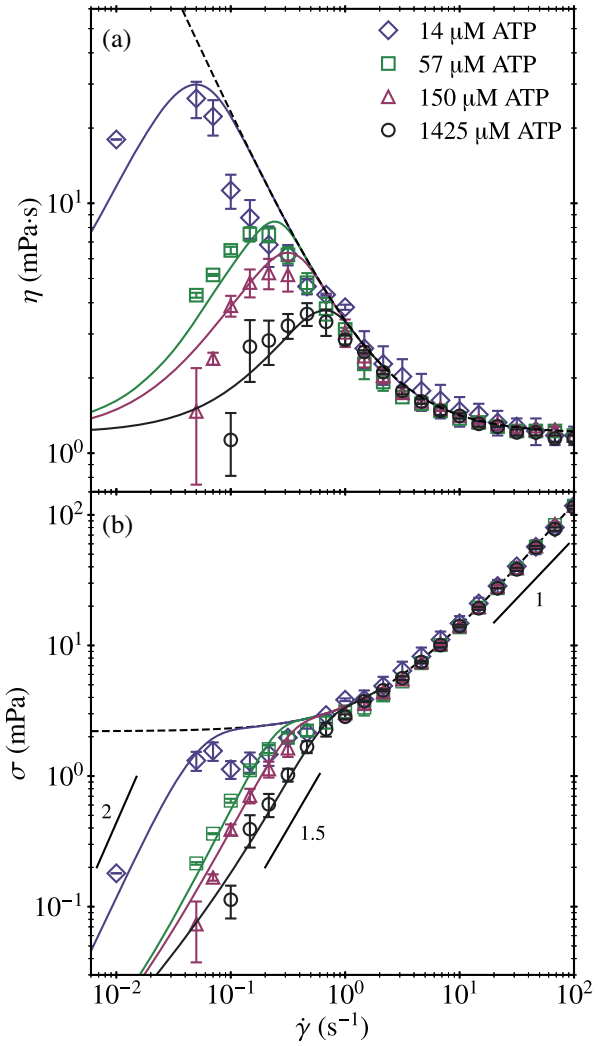

FIG. 3. Modified Bingham plastic model captures rheology of active gels. Rheological measurements (open symbols) for (a) viscosity and (b) stress. Dashed lines represent the Bingham plastic yield-stress model. The solid lines though the data points are from the modified Bingham model, while the labeled lines in (b) provide the power law slopes to guide the eye. At the highest shear rates, the Newtonian plateau must have a $\sigma \sim \dot{\gamma}$, while at low shear rates, $\sigma \sim \dot{\gamma}^{1.5-2.0}$.

The above measurements allow us to quantify the rheology of active networks by extending the Bingham plastic, a model in which the total stress of shear-yielding material is a sum of the viscous and the yield stress: $\sigma = \eta_s\dot{\gamma} + \sigma_y$ [37]. Below $\dot{\gamma}_c$ for all ATP concentrations, the fraction of solidlike elements determines the rheological response by elastically resisting the shear. Unlike conventional *in vitro* biopolymer networks where deformations above the yield strain permanently alter the network

architecture, motor activity continuously reforms the yielded solidlike elements. These solidlike elements contribute to the measured stress at the yield stress of the static gel, σ_y. To account for the solidlike elements within the sheared network we use $C(\dot{\gamma})$ as a coefficient for σ_y. Writing $\sigma = \eta_s\dot{\gamma} + C(\dot{\gamma})\sigma_y$, and $\eta = \eta_s + C(\dot{\gamma})\sigma_y/\dot{\gamma}$ preserves the rheological framework while accounting for the ATP-dependent fraction of solidlike elements. The proposed model has two parameters, the high-shear viscosity, $\eta_s = 1.2$ mPa s, and the yield stress, $\sigma_y = 2.2$ mPa, both of which were independently measured [Figs. 1(d) and 1(e)]. Using these values the model quantitatively describes the rheology of active MT networks for all applied shear rates and ATP concentrations [Figs. 3(a) and 3(b)]. Specifically, we observe two distinct stress regimes with an ATP-independent scaling, $\sigma \sim \dot{\gamma}^{1.5-2.0}$ and $\sigma \sim \dot{\gamma}$; where the transition maps out a set of points that lie along a plateau determined by the static gel yield stress. Solidlike elements, therefore, behave like a static gel, and above $\dot{\gamma}_c$, the growth of the shear stress is dominated by the viscous contribution.

We showed that with decreasing ATP concentration extensile active networks undergo a transition from a fluid to a solidlike state. The location of the transition is dependent on both the intrinsic ATP-dependent dynamics and the externally applied shear rates. Such fluid-to-solid transition is not predicted by existing theoretical models which assume that active stresses monotonically change with ATP concentration [38]. Intriguingly, analysis of instabilities also suggested the presence of solidlike material when the concentration of motor clusters is too low to fluidize the networks [39]. Therefore, extensile microtubule networks represent a distinct class of active matter systems, whose rheological properties are fundamentally different from both suspensions of swimmer-based microorganisms or previously studied contractile active networks [15,17,19,22]. Both microscopic swimmers and MT-based active matter are composed of rodlike particles, however the mechanisms of active stress generation in these two systems is fundamentally different. Microscopic swimmers generate active stress by themselves, thus their suspensions retain some activity in the dilute limit. In extensile networks, the stresses are generated by molecular motors, but only when they link and move a pair of otherwise passive rodlike MTs. Consequently, MT networks are not suspensions but have elastic percolating structures. These microscopic differences are reflected in the fundamentally different rheology of microswimmers and extensile networks. Depending on the sign of the active dipole the microswimmer suspension viscosities can either increase or decrease with activity [18,20,40]. As demonstrated here the rheology of extensile networks is significantly more complex.

It is also worth considering our findings from the perspective of contractile active cytoskeletal networks, which were studied in both actomyosin and MT-kinesin systems [9,10]. Despite extensive efforts, controlling the sign of active stresses remains a challenge [41]. Similar to swimmers, the rheology of contractile networks is also fundamentally different from our measurements [42–45]. Recent efforts demonstrated extensile stresses in 2D actomyosin nematics [46]. We believe that reproducing these dynamics in 3D gels would yield rheological signatures similar to those studied here.

To summarize, we demonstrated that microscopic theories of extensile networks must account for both the solid state found at low ATP concentration and the active stresses that effectively melt this solid network. A potential way toward quantitative microscopic model is rooted in our finding that self-yielding active gels are quantitatively described by a simple phenomenological model comprised of solid- and liquidlike elements, and whose contribution are determined by the relative distributions of internally generated and externally imposed rates. Our results demonstrate the need to extend microscopic models of passively cross-linked networks to include dynamical events that produce structural rearrangements and bond breakage driven by local active stresses as has been described in emerging models [47].

We thank Jeffery S. Urbach, Peter D. Olmsted, Emanuela Del Gado, Bulbul Chakraborty, Sriram Ramaswamy, Cristina Marchetti, and Ivan Krocker for discussions. D. A. G., C. D., and D. L. B. thank the Templeton Foundation Grant No. 57392 and Georgetown University for support. Z. D., R. B., and J. B. were supported by the U.S. Department of Energy, Office of Basic Energy Sciences, through Award No. DE-SC0019733. Preparation of samples was made possible by Grant No. NSF-MRSEC-2011486. We also acknowledge use of the Brandeis biosynthesis facilities supported by Grant No. NSF-MRSEC-2011486.

*Corresponding author.
daniel.blair@georgetown.edu
†Equally contributed to this work.

[1] B. Fabry, G. N. Maksym, J. P. Butler, M. Glogauer, D. Navajas, and J. J. Fredberg, Phys. Rev. Lett. **87**, 148102 (2001).
[2] A. W. C. Lau, B. D. Hoffmann, A. Davies, J. C. Crocker, and T. C. Lubensky, Phys. Rev. Lett. **91**, 198101 (2003).
[3] M. Guo, A. J. Ehrlicher, M. H. Jensen, M. Renz, J. R. Moore, R. D. Goldman, J. Lippincott-Schwartz, F. C. Mackintosh, and D. A. Weitz, Cell **158**, 822 (2014).
[4] D. A. Fletcher and R. D. Mullins, Nature (London) **463**, 485 (2010).
[5] J. Brugus and D. Needleman, Proc. Natl. Acad. Sci. U.S.A. **111**, 18496 (2014).
[6] P. Schwille, Science **333**, 1252 (2011).

[7] J. Prost, F. Jülicher, and J.-F. Joanny, Nat. Phys. **11**, 111 (2015).
[8] D. Mizuno, C. Tardin, C. F. Schmidt, and F. C. MacKintosh, Science **315**, 370 (2007).
[9] G. H. Koenderink, Z. Dogic, F. Nakamura, P. M. Bendix, F. C. MacKintosh, J. H. Hartwig, T. P. Stossel, and D. A. Weitz, Proc. Natl. Acad. Sci. U.S.A. **106**, 15192 (2009).
[10] S. Köhler, V. Schaller, and A. R. Bausch, Nat. Mater. **10**, 462 (2011).
[11] P. M. McCall, F. C. MacKintosh, D. R. Kovar, and M. L. Gardel, Proc. Natl. Acad. Sci. U.S.A. **116**, 12629 (2019).
[12] T. Sanchez, D. T. N. Chen, S. J. DeCamp, M. Heymann, and Z. Dogic, Nature (London) **491**, 431 (2012).
[13] G. Henkin, S. J. DeCamp, D. T. Chen, T. Sanchez, and Z. Dogic, Phil. Trans. R. Soc. A **372**, 20140142 (2014).
[14] M. Alvarado, Joséand Sheinman, A. Sharma, F. C. MacKintosh, and G. H. Koenderink, Nat. Phys. **9**, 591 (2013).
[15] Y. Hatwalne, S. Ramaswamy, M. Rao, and R. A. Simha, Phys. Rev. Lett. **92**, 118101 (2004).
[16] A. Sokolov and I. S Aranson, Phys. Rev. Lett. **103**, 148101 (2009).
[17] D. Saintillan, Exp. Mech. **50**, 1275 (2010).
[18] S. Rafaï, L. Jibuti, and P. Peyla, Phys. Rev. Lett. **104**, 098102 (2010).
[19] S. M. Fielding, D. Marenduzzo, and M. E. Cates, Phys. Rev. E **83**, 041910 (2011).
[20] J. Gachelin, G. Miño, H. Berthet, A. Lindner, A. Rousselet, and E. Clément, Phys. Rev. Lett. **110**, 268103 (2013).
[21] M. C. Marchetti, J. F. Joanny, S. Ramaswamy, T. B. Liverpool, J. Prost, M. Rao, and R. A. Simha, Rev. Mod. Phys. **85**, 1143 (2013).
[22] D. Saintillan, Annu. Rev. Fluid Mech. **50**, 563 (2018).
[23] See the Supplemental Material at http://link.aps.org/supplemental/10.1103/PhysRevLett.125.178003 for information on methods and rheology details, which includes Refs. [24–29].
[24] S. Dutta, A. Mbi, R. C. Arevalo, and D. L. Blair, Rev. Sci. Instrum. **84**, 063702 (2013).
[25] T. Sanchez, D. Chen, S. DeCamp, M. Heymann, and Z. Dogic, Nature **491**, 431 (2012).
[26] M. Castoldi and A. V. Popov, Protein Expression Purif. **32**, 83 (2003).
[27] E. Berliner, E. Young, K. Anderson, H. Mahtani, and J. Gelles, Nature (London) **373**, 718 (1995).
[28] Z. Taylor, R. Gurka, G. Kopp, and A. Liberzon, IEEE Trans. Instrum. Meas. **59**, 3262 (2010).
[29] R. Ewoldt, M. Johnston, and L. Caretta, Experimental challenges of shear rheology: How to avoid bad data, in *Complex Fluids in Biological Systems*, edited by S. Spagnolie (Springer, New York, 2015).
[30] M. J. Schnitzer and S. M. Block, Nature (London) **388**, 386 (1997).
[31] N. J. Carter and R. A. Cross, Nature (London) **435**, 308 (2005).
[32] H. Khataee and J. Howard, Phys. Rev. Lett. **122**, 188101 (2019).
[33] Y.-C. Lin, G. H. Koenderink, F. C. MacKintosh, and D. A. Weitz, Macromolecules **40**, 7714 (2007).
[34] C. P. Broedersz and F. C. MacKintosh, Rev. Mod. Phys. **86**, 995 (2014).
[35] Q. D. Nguyen and D. V. Boger, Annu. Rev. Fluid Mech. **24**, 47 (1992).
[36] V. V. Vasisht, S. K. Dutta, E. Del Gado, and D. L. Blair, Phys. Rev. Lett. **120**, 018001 (2018).
[37] E. C. Bingham, Bull. Bur. Stand. **13**, 311 (1917).
[38] L. M. Lemma, S. J. DeCamp, Z. You, L. Giomi, and Z. Dogic, Soft Matter **15**, 3264 (2019).
[39] A. Senoussi, S. Kashida, R. Voituriez, J.-C. Galas, A. Maitra, and A. Estevez-Torres, Proc. Natl. Acad. Sci. U.S.A. **116**, 22464 (2019).
[40] H. M. López, J. Gachelin, C. Douarche, H. Auradou, and E. Clément, Phys. Rev. Lett. **115**, 028301 (2015).
[41] P. J. Foster, S. Frthauer, M. J. Shelley, and D. J. Needleman, eLife **4**, e10837 (2015).
[42] M. Murrell, P. W. Oakes, M. Lenz, and M. L. Gardel, Nat. Rev. Mol. Cell Biol. **16**, 486 (2015).
[43] T. Gao, R. Blackwell, M. A. Glaser, M. D. Betterton, and M. J. Shelley, Phys. Rev. Lett. **114**, 048101 (2015).
[44] J. M. Belmonte, M. Leptin, and F. Ndlec, Mol. Syst. Biol. **13**, 941 (2017).
[45] D. Needleman and Z. Dogic, Nat. Rev. Mater. **2**, 17048 (2017).
[46] N. Kumar, R. Zhang, J. J. de Pablo, and M. L. Gardel, Sci. Adv. **4**, eaat7779 (2018).
[47] D. Goldstein, S. Ramaswamy, and B. Chakraborty, Soft Matter **15**, 3520 (2019).